Materials Today Sustainability 27 (2024) 100852

Contents lists available at ScienceDirect

Materials Today Sustainability

journal homepage: www.journals.elsevier.com/materials-today-sustainability

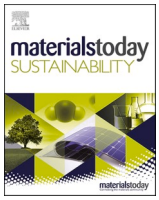

Innovative materials based on physical melt-blending of cutin from tomato waste and poly(lactic acid)

L. Arrighetti [a,b,1], L. Ricci [a,1], C. De Monte [a,*], F. Aiello [a], C.A. Massa [a], F. Balzano [b], G. Uccello Barretta [a,b], S. Bronco [a]

[a] Istituto per i Processi Chimico-Fisici, Sede di Pisa del Consiglio Nazionale delle Ricerche (CNR-IPCF), Via G. Moruzzi 1, 56124, Pisa, Italy
[b] Dipartimento di Chimica e Chimica Industriale, Università di Pisa, Via G. Moruzzi 13, 56124, Pisa, Italy

ARTICLE INFO

Keywords:
Cutin
PLA/Cutin blends
Rheological analysis
NMR analysis
Water vapour permeability
Agri-food waste

ABSTRACT

In the last decades, the improving and the progresses achieved following the principles of circular economy have unveiled virtuous approaches towards environmental challenges regarding the industrial processes. Agri-food waste constitutes a promising starting material for the design of innovative products with a marked improvement of the cradle-to-grave dynamics. In this scenario, the recovery of cutin from tomato peels waste represents an effective example of circular economy.

In this work, the feasibility of the discontinuous melt-blending of cutin with poly(lactic acid) (PLA) was evaluated in order to obtain an innovative green material. Different blends of PLA and cutin have been characterized by using a multi-technique approach (FT-IR, DSC, TGA, SEM, rheological study, water vapour permeability) to achieve information on the nature and properties of these new materials. An important decrease of the final torque of the melt blends was observed, together with a decrease of the melt viscosity. Further increase in the cutin content in the blends was associated to a change in the viscosity of the melt. The addition of cutin to the PLA matrix caused a variation in the water vapour permeability, in accordance with the hydrophobic nature of the cutin.

The obtained results attested that some degradation phenomena occurred along the process; however, the processability of these new blends is not impaired. The potential applications of these materials will mainly concern the agricultural sector and the production of degradable products with low environmental impact.

1. Introduction

According to the European association of plastic manufacturers PlasticEurope, the worldwide plastic production reached 368 million tons in 2019, with 57.9 million tons in Europe [1]. Petroleum-based plastics are typical products of the linear economy paradigm; they are considered as the typical material of the twenty-first century. They are actually ubiquitous and indispensable in everyday life. Despite the widely known advantages of plastic use compared to other materials, multiple problems arising from its massive use are undeniable, especially when plastic waste is dispersed in the environment due to the lack of proper collection and treatment systems. It was estimated that, considering the present trend, by 2040 about 69 million metric tons will be annually disposed of in landfills, and 30 million metric tons of plastics will be discarded in the oceans (1/3 of the value estimated in 2016) due to mismanagement of wastes [2]. Taking into account these numbers, and in order to reduce the entity of the continuous plastic waste accumulation, the development and production of new degradable plastic materials and the partial substitution of petroleum-based plastic on the market may be a practical way to achieve an improvement of the waste management procedures.

One of the possible approaches to achieve the optimization of new plastic composites could be the incorporation of treated industrial waste into polymer matrices classified as biodegradable, such as poly(lactic acid) (PLA). The production of PLA, i.e. of its monomer, from corn starch waste has been already extensively studied [3] owing to its biocompatibility, sustainability and non-toxicity [4,5], and numerous articles report about the use of this waste product in plastic composites production and processing [6]. Poly(lactic acid) is a commercial polyester that is produced generally by ring opening polymerization (ROP) of the

* Corresponding author.
E-mail address: cristina.demonte@cnr.it (C. De Monte).
[1] These two authors contributed equally.

https://doi.org/10.1016/j.mtsust.2024.100852
Received 26 February 2024; Received in revised form 16 May 2024; Accepted 25 May 2024
Available online 25 May 2024

lactide obtained by the condensation of lactic acid from fermentation of corn wastes [7]. PLA has been utilized in various applications such as packaging, automotive components, clothing and medical equipment. However, its inadequate durability, thermal stability, degradation within general environmental condition and oxygen barrier, limit its extensive applications. The preparation of PLA composites with natural and degradable material as fibres [8] or other material from wastes may overcome the shortcomings of this type of plastic. As a consequence, the management of industrial waste could be optimized by avoiding their discarding. The use of food waste for the production of polymer biomaterials responds to the need to limit waste production and to limit the consumption of virgin energy/raw materials and new resources while preserving their use for the growing human population, in line with the principles of the circular economy [9–11]. The UN environment programme reports that the amount of agri-food waste in 2019 [12] was about 931 million tons. In general, this type of waste is generated by processing of fruit and vegetables to obtain final edible products [13] as peeling, core removal and pulping [14]. One of the main problems regarding the potential use of agri-food waste is due to the wide difference between crops species, which involve extreme differences in the chemical composition of the waste resource (content in carbohydrates, protein and lipids as an example) and consequently the need to narrow the options only on one specific line of production for the use of industrial agricultural wastes. The putrescible nature of agri-food industry waste products generated in huge quantities at both the processing and consumption stages (food waste) can give them a high potential to be considered as second raw materials [15]. Horticulture represents the main production in agri-food industry (65%) [16], with about 187 million tons of wastes from the tomato processing as the highest worldwide product in 2021 [17]. The by-products of tomato industry represent the 5–13 wt% on the whole production [18] primarily consisting of peels and seeds. At present, solid wastes from the tomato industry, especially peels, are used as animal feed or for the biogas production. The predominant constituent of tomato wastes consists of fibres (about 25–50%), protein (15–24%), fat (5–20%) and mineral content (4–7%) [19]. Some strategies concerning tomato wastes use are focused on extreme economic valorisation through β-carotenoids and amino acids extraction [20]. Innovative techniques are currently updated along this development line [21] but, in recent years, the attention is more and more focused on fatty acid production by optimizing the quantitative recovery of tomato waste. Fatty acids in tomato wastes are mostly contained in seeds (for example, the extracted seed oil is studied in biofuel applications [22]) and peels, the former essentially containing cutin, polypeptides, phenolics, polysaccharides and minerals. Cutin (Cut), in detail, represents the main component of the cuticular membrane of tomato and plants (about 40–85 wt%).

Cutin is a bio-polyester with chains largely consistent of esterified hydroxylated fatty acids (ω-hydroxylation is very common) and epoxy hydroxylated of the C16–C18 family, mainly 10,16-dihydroxyhexadecanoic acid [23]. The waxy nature of the cutin allows the formation of a defensive membrane impervious to pathogens, able to regulate the water uptake and the transport of nutritional substances [24] in tomato fruits. The presence of different monomeric units inside the polymer chains determines the possibility to have different chemical structures in the cutin network as linear chains or branched chains formed by the reaction between hydroxyl and carboxylic groups. In general, while half of the mid-chain hydroxyl groups in the polymer are involved in cross-link bonds, a large part of the primary hydroxyl groups is involved in ester bonds. As a consequence, there is a very low presence of unesterified carboxyl functional groups [25]. Another possible mechanism established in literature, which contributes to the formation of the chemical structure of the cutin, is the oxidative vicinal diol cleavage reaction. The products of this reaction are dioic acid and hydroxylated acid that contribute to crosslinking [26]. The complex chemical composition of cutin results in a branched, amorphous, and flexible molecular architecture. The 3D network grants interactions with other components of the plant such as waxes, phenolic compounds and polysaccharides [24]. The main features that make cutin interesting for eco-designed application in innovative materials are its non-toxicity, biodegradability, and availability [26]. Despite its ubiquity in terrestrial plants, it has been traditionally underutilized as raw material due to its insolubility, but currently it is used to produce bio-resins and bio-lacquers in food packaging applications, a sort of replication of the cuticular membrane natural functions in plants [27]. More specifically, during the European project called "BIOCOPACplus" [28], funded by "Life+ 2013 Environment Policy and Governance", a pilot plant was built for the extraction of cutin from tomato peels, with a processing simply based on the use of aqueous solution at different pH, for the formulation of eco-sustainable lacquer for coating food-grade metal cans avoiding the use of organic solvents.

In this work, a new possible cutin application was investigated and evaluated by combining its properties with that of extrusion grade poly (lactic acid), obtained from natural resources. Cutin has been separated in its soluble (Cut Ext) and insoluble (Cut Res) fractions through extraction using THF. Both cutin and its fractions have been characterized by infrared spectroscopy (FT-IR), differential scanning calorimetry (DSC), thermogravimetric analysis (TGA) and nuclear magnetic resonance (NMR) spectroscopy, in order to obtain information about their different nature and chemical architecture. Thereafter, composites of PLA and cutin, at different loading of cutin (5-10-20 wt%), have been prepared using Brabender-type discontinuous mixer by melt blending. These blends were thoroughly characterized by using a multi-technique approach to achieve information on the nature and properties of these new materials. In particular, the powders obtained by the grinding of the blends were characterized through FT-IR, thermal analyses DSC and TGA, and gel permeation chromatography (GPC), in order to quantify the entity of possible degradation phenomena due to the processing conditions. With the aim of optimizing the blend processing of these composite materials PLA/cutin, another series of blends has been prepared by using PLA and introducing a pre-grinding step for the cutin component (Mac). The same multi-technique approach was used for the characterization of the second series of blends. After this preliminary characterization, films have been prepared using a hot melt pressing process, and they have been observed macroscopically and microscopically by using a scanning electron microscope (SEM) to notice the possible presence of inhomogeneity and to clarify the possible interaction between polymer matrices in blends. Furthermore, the water vapour transmission rate (WVTR) and the water vapour permeability of each film have been evaluated according to ISO 2528:2017 in order to evaluate the effect of the addition of an hydrophobic material like cutin to PLA also considering possible cutin agglomerates.

2. Materials and methods

2.1. Materials

The cutin was extracted in the pilot plant of "*Azienda Agricola Chiesa Virginio*", Canneto sull'Oglio (MN, Italy). The pilot plant was realized thanks to the European project "BIOCOPACplus" that was focused on the production of bio-laques from organic wastes in collaboration with SSICA (Stazione Sperimentale per l'Industria delle Conserve Alimentari, Parma, Italy), CFT S.P.A. (Parma, Italy) and Salchi Metalcoat srl (Burago di Molgora, Italy). Cutin was maintained frozen, as received, to avoid and/or slow down the degradation phenomena until processing. The water uptake, certified by the pilot plant, was 35 wt% (further confirmed after freeze drying). PLA Ingeo 2003D, grade for thermoforming and extrusion processes with a nominal melting temperature ranging between 145 °C and 160 °C, and a glass transition temperature between 55 °C and 60 °C, was purchased by Natureworks LLC (Minneapolis, Minnesota). Tetrahydrofuran (reagent grade, ≥99.0% + 250 ppm of BHT as inhibitor) and chloroform (HPLC grade, ≥99.8%), provided by Sigma-Aldrich (St. Louis, Missouri), have been used as received

for the fractionation of cutin and for the solubilization of sample blends for GPC analysis, respectively. Deuterated chloroform ($CDCl_3$ 99.8%) and deuterated dimethylsulfoxide (DMSO-d_6, 99.8%) were purchased from Merck KGaA (Darmstadt, Germany) and Deutero GmbH (Kastellaun, Germany), respectively, and were used for the NMR analysis of Cut Ext.

2.2. Cutin extraction

Cutin extractions were carried out on about 1 g of ground cutin using a total amount of 150 mL of THF [25] with 3 consecutive extractions (50 mL each) at room temperature in a glass flask for 4 h in the first two steps and about 16 h in the third one. A transparent yellow-brown coloured solution was obtained together with a dark brown solid (insoluble components Cut Res). The two fractions were separated by centrifugation at 10000 rpm for 10 min. The yellow supernatant phase was collected and the solvent was removed by rotavapor (Cut Ext).

2.3. Preparation of the sample blends and films

Cutin was lyophilized using Pascal-LIO 5PDGT in order to remove adsorbed water at −50 °C and 0.01 mbar for two days. PLA Ingeo 2003D pellets were pre-dried at 80 °C for 8 h in a vacuum-oven to remove the humidity absorbed. Mac was prepared from lyophilized cutin by using the mechanical grinder IKA A11 basis to obtain finer grains. The sample blends were prepared by using the discontinuous mixer Brabender-type Plastograph EC, with a mixing chamber of 30 cm^3, interfaced with Brabender Mixing Software "Win Mix 1.0" for the data management and acquisition. All the blends were processed at 50 rpm for 10 min at 180 °C. The larger part of the defined and weighted amount of PLA pellets was added at the beginning of the mixing, and after the start of the Torque registration (estimated as the moment of practically complete melting of PLA pellets) cutin was added to the process with calculated weight ratios ranging between 5 wt% to 20 wt% with respect to the total mass of sample in the mixing chamber (approximately 30 g). After the addition of the cutin/Mac, the remaining PLA was finally added into the mixing chamber and maintained closed until the end of processing. At the end of the processing each blend was collected and ground using the mechanical grinder IKA MF 10 B with a septum of 1 mm. Sample films were prepared by compression moulding by using a Carver No3851CE hot melt hydraulic press. About 1 g of each sample was placed between two Teflon sheets and placed between two plates preheated at 180 °C. Each sample was subjected to a pressure of 1 ton for 1 min and then to a pressure of zero tons for 2 min at the same temperature.

2.4. Characterization methods

All FTIR analyses were performed with "Jasco FT/IR6200" spectrometer. All the samples underwent 128 scans from 4000 to 650 cm^{-1} for Attenuated total reflection (ATR) analyses (using the ATR accessory PIKE MIRacle equipment).

The NMR analysis was performed on a VARIAN INOVA600 spectrometer equipped with a 5 mm reverse probe operating at 600 MHz and 150 MHz for ^1H and ^{13}C nuclei, respectively. The proton and carbon chemical shifts were referred to tetramethylsilane (TMS) as the external standard, and the temperature was controlled to 25 ± 0.1 °C through the Varian control unit. Proton (^1H) spectra and 2D experiments were performed by using the minimum spectral width required. ^1H NMR experiments were performed by using a relaxation delay of 10 s, a 90° pulse of 9.3 μs, 128 scans, and a receiver gain of 20. The gCOSY (gradient COrrelation SpectroscopY) maps was recorded by using a relaxation delay of 1 s, 256 increments of 64 transients, and 4 K data points. The TOCSY (TOtal Correlation SpectroscopY) maps were recorded by using a relaxation delay of 1 s, 256 increments of 64 transients, 4 K data points, and a mixing time of 80 ms or 120 ms. The ROESY (Rotating-frame Overhauser Enhancement SpectroscopY) maps were recorded by using a relaxation delay of 1 s, 256 increments of 64 transients, 4 K data points and a mixing time of 300 ms or 500 ms. The gHSQC (gradient Heteronuclear Single Quantum Correlation) experiment was recorded with a relaxation delay of 1.2 s, 200 increments, 64 transients, and 2 K data points. The gHMBC (gradient Heteronuclear Multiple Bond Coherence) experiments were recorded with a relaxation delay of 1.2 s, 200 increments, 64 transients, 2 K data points, and by choosing the following values for the long-range coupling constant: 3 Hz, 8 Hz and 12 Hz. Diffusion Ordered SpectroscopY (DOSY) experiments were carried out by using a stimulated echo sequence with self-compensating gradient schemes and 64 K data points; typically, g was varied in 15 steps (64 transients each) and Δ and δ were optimized to obtain an approximately 90–95% decrease in the resonance intensity at the largest gradient amplitude. After data acquisition, each free induction decay (FID) was apodized with 1.0 Hz line broadening and Fourier transformed. The baselines of all arrayed spectra were corrected prior to processing the data. The data were processed with the DOSY macro (involving the determination of the resonance heights of all of the signals above a pre-established threshold and the fitting of the decay curve for each resonance to a Gaussian function) to obtain pseudo-2D spectra with NMR chemical shifts along one axis and calculated diffusion coefficients along the other axis.

About 20 mg of Cut Ext were dissolved in 1 mL of $CDCl_3$. The undissolved portion was removed and the solution was transferred into the NMR tube for the analysis.

DSC experiments were performed on cutin and its fractions with a "Seiko SII ExtarDSC7020" calorimeter according to the following thermal protocol in hermetically closed sample pan: first cooling step from 20 to −60 °C (hold 5 min); first heating step from −60 to 150 °C (hold 5 min); second cooling step from 150 to −60 °C (hold 5 min); second heating step from −60 to 150 °C (hold 5 min); third cooling step from 150° to −60 °C (hold 5 min); last heating step from −60 to 20 °C (not registered). The cooling/heating rate was always 10 °C/min except for the last heating process, when it was fixed to 30 °C/min. The thermal protocol for polymer blends in open sample pan was: first heating step from 20 to 200 °C; holding step at 200 °C for 1 min; second cooling step from 200 to −50 °C; holding step at −50 °C for 3 min; second heating step from −50 to 200 °C; holding step at 200 °C for 1 min; third cooling step from 200 to 20 °C (not registered). The cooling/heating rate was always 10 °C/min except for the last cooling process, when it was fixed to 40 °C/min. The sample amount used was about 5 mg in all cases. The degree of crystallinity (χ%) of polymer blends was estimated by using equation (1):

$$\chi\% = \frac{|\Delta H_m + \Delta H_{cc}|}{\Delta H_m^{\circ}} * \frac{100}{x} \quad (1)$$

where x is the weight percentage amount of PLA in polymer blends, ΔH_m and ΔH_{cc} are the measured melting enthalpy and the cold crystallization enthalpy of samples, respectively, and ΔH_m° is the theoretical melting enthalpy value of 100% crystalline PLA (93.6 J/g [29]) with the aim of excluding the contribution of the crystals formed during cold crystallization.

TGA was performed by a "SII TG/DTA 7200 EXSTAR Seiko" analyser under nitrogen inert atmosphere fluxed at 200 mL/min during all measurements from 30 to 700 °C at a 10 °C/min rate in alumina pan. The samples of cutin and its fractions (Cut Res and Cut Ext) were previously freeze-dried before the measurement as the considerable quantity of water absorbed did not allow the analysis to be successful (the sample swelled in the pan).

Scanning Electron Microscope (SEM) images were recorded with the FEI Quanta 450 ESEM FEG electron scanning microscope operating at CISUP Laboratories of University of Pisa. Specimens have been prepared by cryogenic fracture of PLA blends performed by immersion of a piece of each film in liquid nitrogen for 4 min and quickly cut by cooled

scissors.

PLA blends were analysed by gel permeation chromatography using HPLC "Agilent 1260 Infinity" equipped with a three-way valve as injection system, a styrene-divinylbenzene resin as stationary phase and a refractometric detector. The operating pressure was 80 bar and $CHCl_3$ was used as eluent at 0.3 mL/min of flow. Solutions were prepared by dissolving the materials in $CHCl_3$ with a concentration of 2 mg/mL and filtered two times with an Agilent filter with a porosity of 2 μm.

Rotational Rheometer Anton Paar *"MCR302"*, interfaced through dedicated software Rheoplus3.62 was used. The instrument is equipped with two flat parallel plates (diameter of 24.992 mm, default measuring position gap 1 mm). Tests were carried out in oscillatory mode at constant temperature (175 °C) at a fixed strain of 3% and in a frequency range between 0.01 and 100 Hz with five point per decade in linear regime. For each sample the measure was repeated three times.

Water vapour permeability was measured using a XS/Pro-PermeH2O Extrasolution. Sample films were prepared through hot melt pressing with thickness between 100 and 200 μm. Each thickness value was measured with a micrometer "Caliper". The surface of films tested was 50 cm^2. For the permeability measure, before each test starts, the instrument conditions each sample for 8 h at 23 °C and relative humidity of 50% on the permeant side while the other side was dried during the conditioning (ISO 2528:2017). The gas carrier was dried nitrogen steam with a flux set to 11.80 mL/min. Water vapour concentrations within the nitrogen steam was measured by an infrared detector equipped to the instrument. Each analysis was considered finished when the water vapour transmission rate (WVTR) remained constant when the signal variations were inferior to 0.5% of the average value (stability level). The measurement was repeated three times for each analysed sample.

3. Results and discussion

3.1. Cutin and its fractions characterization

Lyophilization of wet samples of cutin was used as the first analytical valuation. The water uptake of 34.5% in the total mass of cutin resulted similar with the declared value by the producer. Secondly, in order to ascertain the presence of different nature of cutin fractions it was chosen to separate its soluble (Cut Ext) and insoluble part (Cut Res) through THF fractionation [30] (Fig. 1).

The yellow colouring (Fig. 1 middle) of the obtained solution attested the solubilization of a cutin's fraction (Cut Ext). The insoluble residue (Cut Res) was separated by centrifugation and it appeared as a gummous dark brown solid (Fig. 1 right). The amount of soluble and residual parts was estimated to be 69% ± 5% and 31% ± 5%, respectively.

IR spectra were obtained using FT-IR ATR analysis, due to the impossibility of solubilizing Cut Res in a suitable solvent. The spectra (Fig. 2) were normalized using the CH asymmetric stretching band at 2928 cm^{-1} (marked with * in Fig. 2).

The bands of cutin were assigned as the following: 3295 cm^{-1} as the absorption of the –OH stretching, 2928 and 2854 cm^{-1} as the asymmetric and symmetric stretching of the aliphatic CH respectively, 1704 cm^{-1} as the stretching of the carbonyl group related to free acid groups, 1639 and 1604 cm^{-1} as double bonds and conjugated double bonds C═C (see inset). The presence of bands at 1515 and 1454 cm^{-1} was considered as a possible indication of presence of aromatics groups, whereas a band at 1170 cm^{-1} was assigned to the C–O stretching of the ester group [31]. The decrease in the intensity of the –OH band at 3295 cm^{-1} after the extraction with THF (Cut Res) is probably due to the reduction of the water uptake due to the extraction. The spectra of Cut Res showed the presence of a band at 1725 cm^{-1}, present as only a slight shoulder on Cut Ext and on raw cutin (Cut) spectrum [32]. This band is associated to the C═O stretching mode of the ester group and could be a possible indication of the marked crosslinked nature of the residue fraction [31,33].

DSC experiments were carried out in a closed aluminium sample pan to avoid the evaporation of the water, in order to highlight any phase transitions in the cutin. It was chosen to report the first and the second heating to better evaluate the real composition of raw cutin and its fractions after the removal of thermal history effects on material (Fig. 3 and Table S1 in Supporting Information).

Cut and Cut Ext showed, respectively, a wide melting peak at a temperature slightly higher than 60 °C as observed by Benítez et al. [34], this peak is split and little lower than 50 °C in Cut Ext. The differences of behaviour between the two samples may be due to the different nature of cutin fractions [35]. Cut Res, on the other hand, which is supposed to consist of a crosslinked and hindered network, does not show melting.

In both heating processes Cut Ext showed the lower glass transition temperature (T_g) value, Cut Res showed the highest, while the raw material Cut showed intermediate values, as expected. All T_g temperatures are observed below zero Celsius. The T_g values were consistent with those reported by Benítez et al. [36].

The thermal stability of cutin raw material and its fractions was determined by TGA analysis under nitrogen atmosphere on lyophilized samples. For this reason, it was not possible to estimate the quantity of

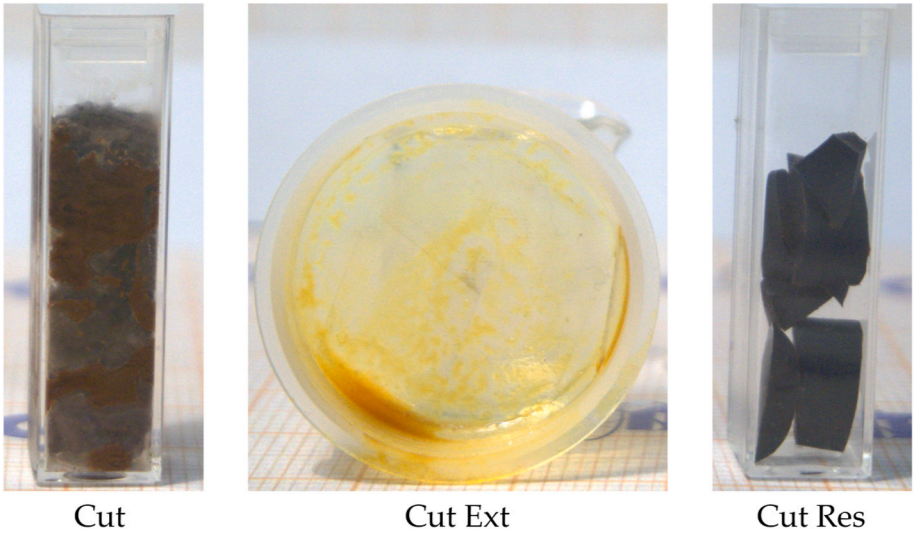

Fig. 1. Cutin (left) and its fractions: Cut Ext (middle) and Cut Res (right). It is worth noting that the content of cutin shown in the three pictures does not represent the quantitative ratio between the components.

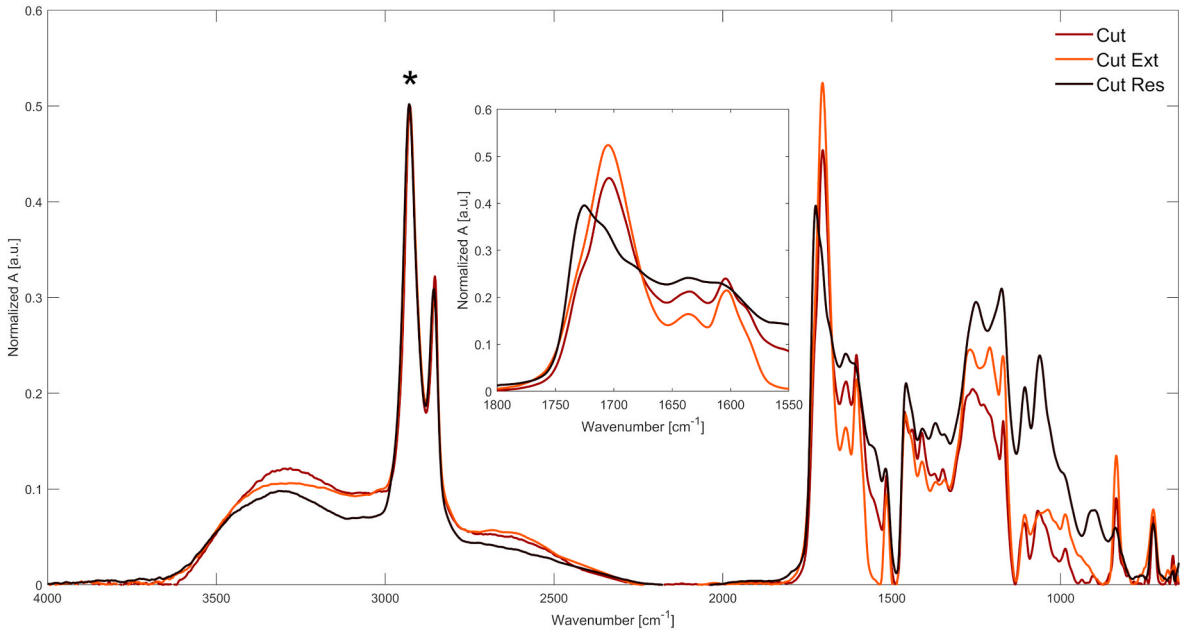

Fig. 2. FT-IR ATR spectra of Cut (brown line), Cut Ext (orange line) and Cut Res (dark brown line). In the inset, the enlargement of carbonyl and double bond stretching zone. * Shows the band used for the normalization. (For interpretation of the references to colour in this figure legend, the reader is referred to the Web version of this article.)

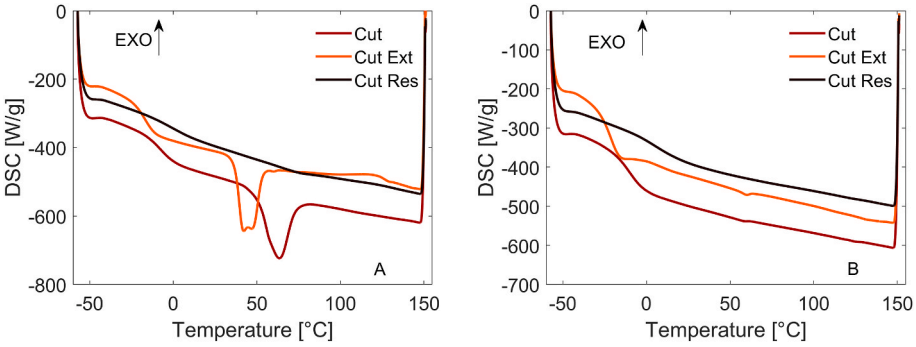

Fig. 3. First heating (A) and second heating (B) DSC curves of Cut, Cut Ext and Cut Res.

water present in the samples. All samples were thermally stable up to 150 °C. Both raw and extracted cutin showed a first weight loss between 200 and 300 °C (this phenomenon was less detectable on the insoluble cutin profile). These peaks are common and mostly associated to the dehydration and decarboxylation processes of the hydroxyacids, absent in Cut Res indicating high esterification degrees [26,37]. The main mass losses, observed in the thermograms in the range between 400 and 500 °C, are comparable with that of 10,16-dihydroxyhexadecanoic acid, which is the precursor of the cutin main monomer unit. This phenomenon was already described in the characterization of a series of homopolymer of poly-hydroxylated fatty acid [26] with a similar even if simpler chemical structure of cutin. It is reported that the trend between 400 and 500 °C seems to be similar to the decomposition pattern observed for estolides from acid oils that may be due to fragmentation of

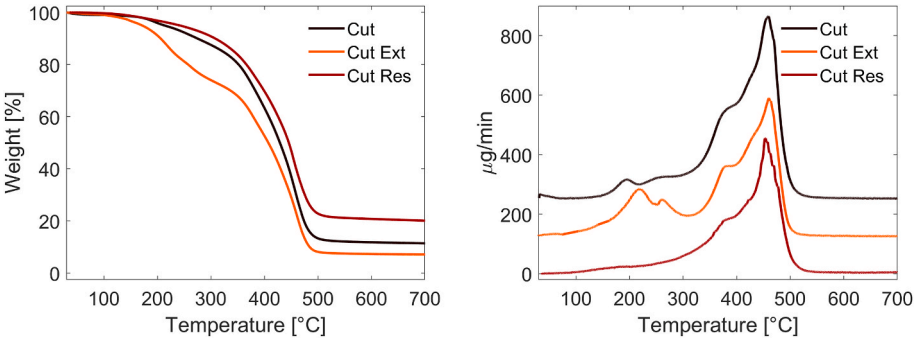

Fig. 4. TGA (left) and DTG (right) curves of Cut, Cut Ext and Cut Res.

the aliphatic chains of fatty acids [38]. The main thermo-degradation mechanism could be then related to the ester bonds splitting into olefin and carboxylic acid, followed by the degradation to CO_2 and water. However, from these observations and from the large number of degradation steps evidenced by the peaks in the thermograms first derivative, the heterogeneity of the cutin matrix was apparent. The TGA profile (Fig. 4) of Cut Ext (orange line) was totally shifted to lower temperatures with respect to that of raw material (brown line), consistently with the observations already made on DSC analysis. Moreover, the Cut Res (dark brown line) showed a profile totally shifted to the highest temperatures, compatible with its crosslinked nature. The relevant temperatures from each TGA and DTG profiles, reported in Table S2 in the Supporting Information, show that Cut Ext had the lowest starting temperature of degradation (T_{onset}), Cut Res the highest while the raw material started to degrade at intermediate temperature.

The NMR analysis of the cutin extract was performed in $CDCl_3$, even if not all the solid was dissolved by this solvent. Deuterated dimethylsulfoxide (DMSO-d_6) was able to completely solubilize the cutin sample, but the water signal, that in this solvent is centred at 3.32 ppm, overlapped with a diagnostically very important spectral region. Considering that the spectral profiles in the two solvents are comparable, and that the insoluble fraction in $CDCl_3$, once dissolved in DMSO-d_6, did not produce additional signals, deuterated chloroform was preferred for the NMR analysis.

The soluble portion of Cut Ext was thoroughly analysed by combining 1D and 2D experiments that allowed identifying most of the species present in solution. In particular, low molecular weight components, such as γ-butyrolactone and *p*-coumaric acid, together with fragments of fatty acids similar to linoleic/linolenic chains, and a macromolecular structure mainly composed by C16 alkyl chains were identified (see Supporting Information for further details). Fig. 5 summarized the NMR findings.

3.2. Polymer blends: preparation and characterization

PLA, PLA/Cut and PLA/Mac blends were prepared in a discontinuous mixer Brabender type according to the reported setup, with a concentration of cutin (Cut) and ground cutin (Mac) increased from 5% to 20 wt % and from 10 wt% to 20 wt%, respectively. The trends reported in Fig. 6 (the values of final Torque are reported in Table S4 of Supporting Information) clearly indicated a marked decrease of final torque by increasing the cutin content. The effect could be due to the degradation of the polymer matrix or a plasticizer effect, both due to the cutin. The reduced granulometry of ground cutin could cause a minor stress on PLA matrix under processing conditions. At the same concentration, the final torque of the sample with ground cutin was higher than the unground one.

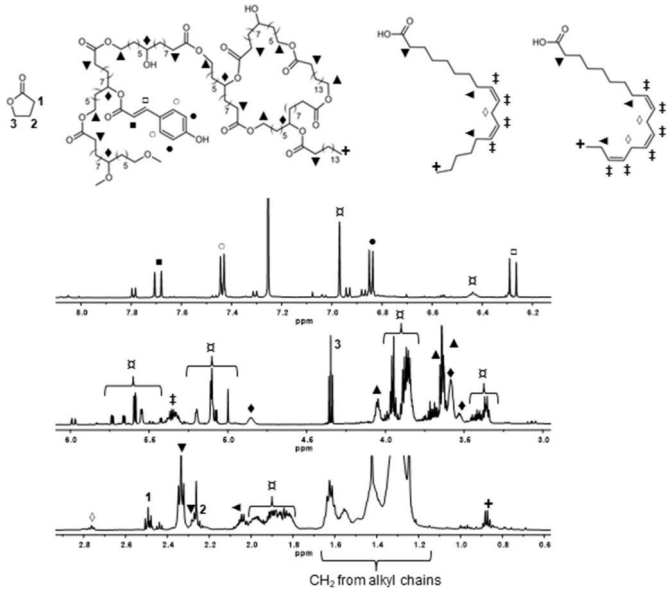

Fig. 5. ^{1}H NMR (600 MHz, $CDCl_3$, 25 °C) spectrum of Cut Ext with the structures hypothesized on the basis of the NMR analysis; ¤ indicates the proton signals belonging to structures not yet identified.

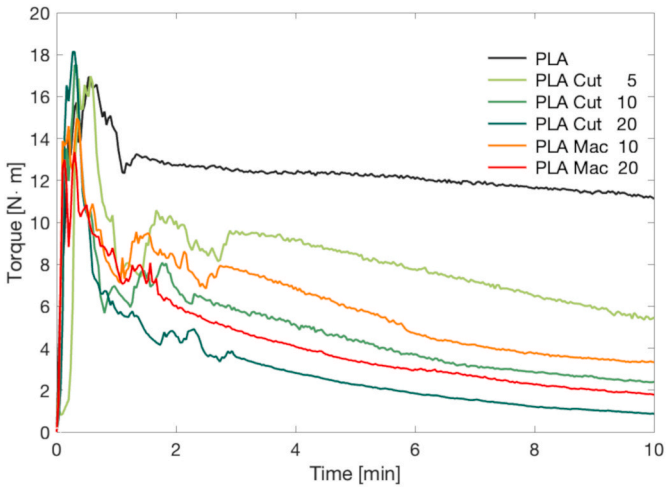

Fig. 6. Torque profiles of PLA, PLA/Cut and PLA/Mac blends.

The increase in cutin content gives rise to a shift to lower values of the molecular weight distributions of PLA fraction with higher retention time (see Fig. S6 in Supporting information). The use of ground cutin caused a less marked degradation of PLA. Furthermore, a slight increase in the polydispersion was observed with the increase in the cutin content, consistently with the degradation tendency of the polymer matrix (Table 1, PLA Cut10 *vs*. PLA Mac10 and PLA Cut20 *vs*. PLA Mac20).

The molecular weight distribution of PLA Mac10 was shifted to higher values than that of PLA Cut10, probably because smaller aggregations remain in melt-blending of ground cutin and this may contribute to a lower extent of the degradation of PLA matrix. Similar variations were observed between PLA Cut20 and PLA Mac20. The amount of cutin plays an important role on the reduction of the molecular weight of PLA: increasing the amount entails a larger reduction of the molecular weight, probably due to the increase of the share stress inside the mixing chamber for the presence of aggregates as already stated on Torque analysis.

Rheological tests were conducted on frequency sweep between 0.01 and 100 Hz in the linear regime (previously evaluated for each sample on the same operating conditions) at 175 °C and at constant strain of 3% with a gap of 1 mm. The complex modulus of viscosity was measured by the instrument with 5 points per decade. In general, polymer materials can show viscoelastic response to stress and strain, a complex combination of purely elastic and purely viscous behaviour. Therefore, these dynamics have heavy consequences on the processability and performance of the materials, especially when they undergo to extrusion processes. All the samples show a decrease of complex viscosity as the

Table 1
Average and Ponderal Molecular Weight of analysed blends and related polydispersity index. The error in the measurements is ±5% for all the data.

Samples	$\overline{Mn}$ (kDa)	$\overline{Mw}$ (kDa)	PD
PLA	115.5	126.1	1.1
PLA Cut5	75.8	101.0	1.7
PLA Cut10	52.4	98.9	1.9
PLA Cut20	31.9	67.0	2.1
PLA Mac10	71.1	121.0	1.7
PLA Mac20	52.4	82.9	1.6

frequency increases. The reference shows the typical shear thinning behaviour of commercial PLA with an initial plateau at $3.8 \times 10^6\, mPa * s$ [39], while Cut and Mac blends show radically different trends (Fig. 7) in particular at low frequency (solid-like behaviour zone). The complex viscosity modulus curves of PLA Cut5, PLA Cut10 and PLA Mac10 shifted at lower values than that of the reference, consistently with molecular weights measured by GPC, and its variation seemed to be sharper than that of the reference as the frequency increased. The samples with the highest cutin content, PLA Cut20 and PLA Mac20, showed higher values than the reference at low frequency in the solid region η* and then decreased sharply at high frequency. This significant variation in the viscoelastic behaviour of the composites can be associated with the presence of a three-dimensional network [40,41]. The crosslinked fraction in the blend, which essentially remained in the solid state, caused the increasing of complex viscosity modulus at low frequency with respect to that of all other samples until the degradation occurred. Furthermore, as the addition of cutin increased, the decrease in |η*| becomes more pronounced (stronger shear thinning behaviour) consistently with the torque values finally observed at the end of the Brabender processing. This trend may be attributed to molecular weight loss [42] or to the cutin crosslinked network break up that reinforces the power-law relation between complex viscosity and frequency [40,43].

To better understand the effect of the different Cut/Mac concentrations in the blends on the complex viscosity dependence on frequency, each sample curve was analysed by Carreau-Yasuda model (Fig. 8). The Carreau-Yasuda model relates the complex viscosity to zero complex viscosity, power-law index, relaxation time, shear stress and the range of the transition between the Newtonian behaviour and the power-law behaviour according to equation (2):

$$\eta^*(\omega) = \eta_0^* * \left[1 + \left(\frac{\eta_0^*}{\tau^*} * \omega\right)^{\alpha}\right]^{\frac{n-1}{\alpha}} \quad (2)$$

where η_0^* is the zero complex viscosity, τ^* is the shear stress at the transition from Newtonian to power law trend, ω is the frequency, n is the power-law index and α quantifies the width of the transition from Newtonian to power law trend. Equation (2) can be used considering that η_0^* can be approximated to the complex viscosity value at very low frequency, and the relaxation time can be considered as the ratio between η_0^* and τ^*. In particular, it was chosen to fit the curve in the range from 10 rad/s to 10^3 rad/s, where the observed behaviour was assumed more similar to the reference, in order to highlight deviations from the model.

The Carreau-Yasuda model seemed to consistently describe the rheological behaviour of poly(lactic acid) within the studied frequency range. For the blends instead, it is possible to observe that the model consistently fit the curves only between 10-10^3 rad/s but it was not descriptive at the lowest values in the solid-like region. According to literature [44] these deviations may be due to the entanglements between PLA and other different chains (cutin in this case). In particular, the droplets of melt cutin and especially the solid particles of its crosslinked fraction dispersed in the melt PLA during the measurements, could potentially cause increasingly more entanglements, thus causing deviations from the model.

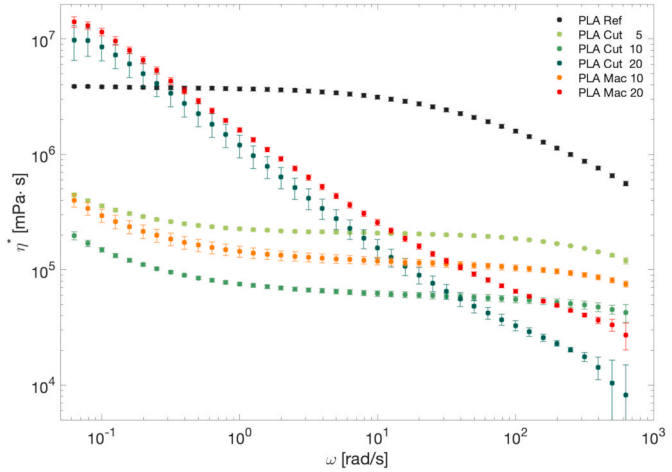

Fig. 7. Complex viscosity trend of the samples as function of frequency.

To analyse the homogeneity of the samples, films produced by hot melt pressing were prepared. As shown in Fig. 9, differences on the texture and form of the films can be attributed to cutin addition. Films made by PLA (black square) appeared to be homogeneous, transparent and with circular margin while those made by PLA/Cut and PLA/Mac blends appeared transparent only at lower cutin content (≤10 wt%), with a more irregular margin. The addition of cutin caused the progressive brown colouring of the films. Cutin agglomerates were clearly apparent in each case, but their presence seemed to further increase at a higher percentage and seemed to be reduced by grinding cutin. Blends with ground cutin produced films with better shape. This fact is not necessarily a problem for the use of this type of material, but it must be considered in the perspective of potential future applications.

SEM images (Fig. 10) of the cryogenic fracture of PLA showed a smooth surface, whereas roughness increased in the blends. The agglomerates were concentrated especially at the edge of the fracture near to the surfaces of the films. Cutin also seemed to have a plasticizer effect on the PLA matrix. The reduction of the sizes of the cutin agglomerates induced by grinding is shown in Fig. 10 consistently with the macroscopic observation done on film surfaces (Fig. 9).

Concerning thermal analyses (TGA), both PLA and the blends showed their main mass loss between 300 °C and 400 °C even if all the blend profiles were shifted to lower temperatures than the reference (Fig. 11 and Table 2). Despite this shift towards lower degradation temperatures, the onset temperature remained above the common processing temperature required for PLA (180–200 °C) thus indicating their possible use in similar conditions. The T_{onset} difference among the reference and the blends appeared to be consistent with the cutin addition but it is not proportional to its amount in the blends. In particular, T_{onset} of PLA Cut5 is shifted 30 °C below the reference's value, while at higher cutin content (both at 10 and at 20 wt%) the shift remains constant to about −50 °C below the reference. These results suggest that the degradation starts at lower temperature, but proceeds at the same speed. Consistently with the investigation of the thermal behaviour of cutin, another mass loss, centred between 400 °C and 500 °C, was observed and attributed to the added cutin in the blends. All these considerations are consistent with the GPC analysis, which highlighted the decreasing of the molecular weight.

The calorimetric properties of the PLA matrix resulted affected by the addition of cutin with major evidence in increasing of the cutin content (Table 3).

The glass transition temperature of PLA slightly decreases as the amount of cutin increases, up to a maximum variation of −5.5 °C with a PLA Cut20.

In the thermograms of the blends with a cutin content higher than 5 wt%, it was possible to observe the glass transition of the cutin shifted to temperatures higher than the T_g of the raw cutin (magnification 1 in Fig. 12).

The presence of cutin shifts the cold crystallization maximum of the blends towards higher values and increases the degree of crystallinity. The increase in the crystallinity degree is more marked as the quantity of cutin increases. At the same cutin concentration, samples with ground cutin have the highest T_{CC}. An obstacle to the movement of the chains during the heating process could be the explanation of these behaviours.

In the PLA melting range of temperatures, only one melting peak is present for raw PLA and PLA with 5% cutin, while two typical peaks appear for the composites with a higher cutin content, which are due to the two different crystalline forms of PLA form α and form α'. Blends

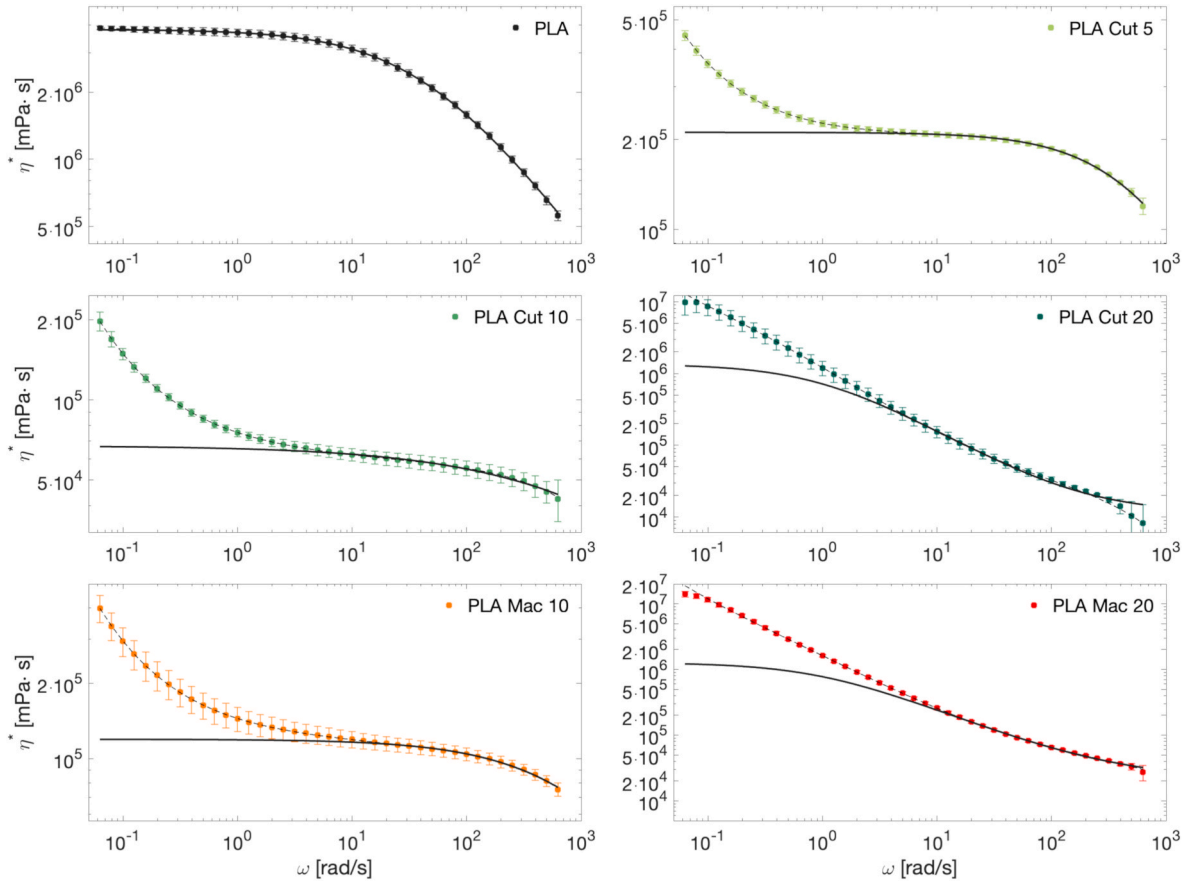

Fig. 8. Carreau-Yasuda model compared to each sample experimental behaviour.

samples with different cutin treatments (Cut or Mac) show differences in the shape of the thermal profiles of the two melting peaks. For the PLA/Cut blends there is a particularly apparent splitting of the peaks, while for the PLA/Mac blends the peak assigned to the α-form of PLA appears as a shoulder of that assigned to the α′-form. The melting temperatures of the α-form in the profiles of the PLA/Mac blends are slightly higher than those of the PLA/Cut blends, thus showing a higher stability of the materials ensuing from the lower processing thermo-mechanical stress. Generally, the melting temperatures of the blends are slightly lower than those of pure PLA.

These observations may be ascribed to specific interactions between PLA and cutin. The complex nature of cutin presented a soluble part of linear and branched esters with differently oxidized functional groups and an insoluble crosslinked matrix of polyesters. The soluble fraction of cutin may act as plasticizer while the insoluble one may both hinder the chain movement during crystallization or act as nucleating agents for the formation of crystal nuclei. Water vapour permeability analyses were carried out on films of PLA and blends. Generally, compostable/biodegradable polymers have relatively high-water vapour permeabilities given their relatively higher polarity, and relatively higher values of water vapour solubility than that of polymers as PE, PP and PET [45]. In general, water permeability in polymer films is dominated by the solubility of water in the polymer and by the crystallinity of the polymer structure and its glass transition temperature [46]. In particular, the permeation phenomenon is closely related to the size of the permeating molecule and to the response of the film to its passage. Above the T_g the polymer chains of the amorphous regions have enough energy to move so that the permeation is easier than below the T_g. As for the crystallinity, crystal domains act as impervious obstacles to the diffusion of water forming a series of "tortuous paths" for its passage in the amorphous phase [47].

In order to compare the WVTR values of the individual analysed samples, it is necessary to normalize the measurements. For this purpose, an average thickness of 0.12 mm for the films examined was chosen and used in equation (3):

$$WVTR_{i(n)} = \frac{WVTR_i * t_i}{0.12} \tag{3}$$

where $WVTR_{i(n)}$ is the water vapour transmission rate normalized value, $WVTR_i$ is the measured value, and t_i is the film thickness (in mm) calculated as the average value of the thickness measured on three points of the film [48].

Permeability values (P_i) were obtained by $WVTR_i$ and t_i using equation (4):

$$P_i = \frac{WVTR_i * t_i}{\Delta p_i} \tag{4}$$

where Δp_i is the gradient in partial pressure of water measured in mmHg.

It is important to observe that possible hydrolysis reactions should also be considered to interpret the results of these measurements. PLA undergoes hydrolysis reactions in which the ester bonds are cleaved, and molecular weight is reduced, but this process is accelerated only by catalytic action of enzymes. In another work, which investigates the kinetics of PLA hydrolysis at 90% relative humidity in a range of temperature between 20 °C and 50 °C, it was demonstrated that hydrolysis mechanism is a very slow process compared to that of water vapour permeation [49]. Fig. S7 in the Supporting Information reports trends of the $WVTR_{(n)}$, the numerical values at 23 °C and relative humidity of 50% are reported in Table 4.

A one-way ANOVA test ($p = 0.05$) followed by a post-hoc Tukey's test was carried out to attest the significance of the WVTR and water vapour permeability variations observed compared to that of the PLA

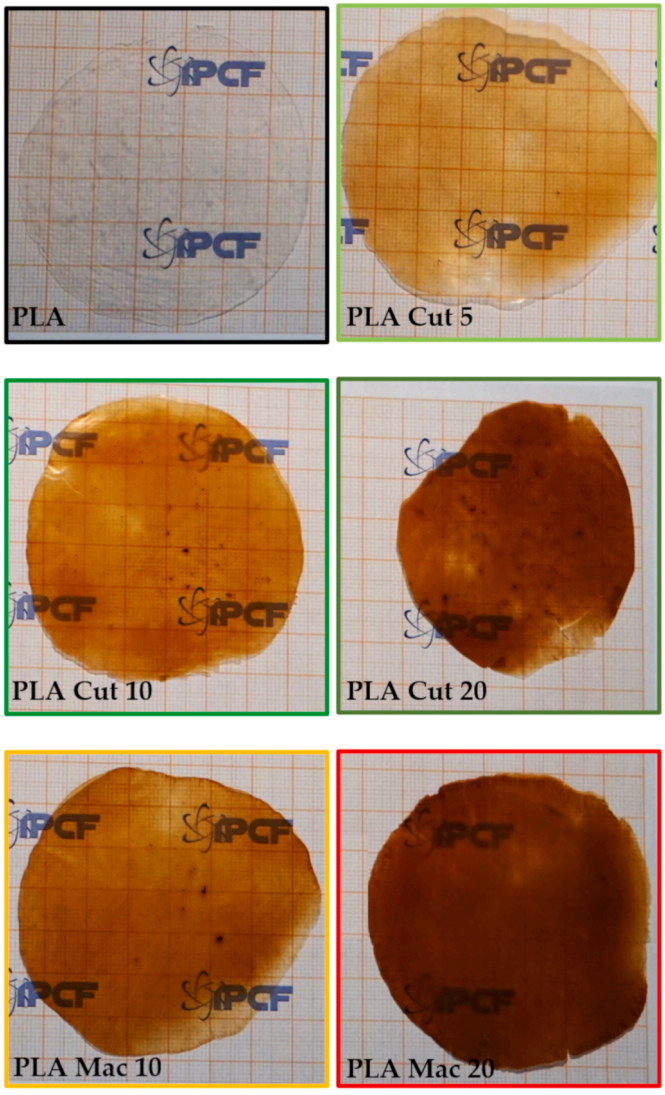

Fig. 9. Films made by PLA, PLA/Cut and PLA/Mac blends through hot-melt hydraulic pressing.

alone. It is possible to state that the addition of cutin, consistently with its waxy nature, causes a significant decrease of the water vapour transmission rate (Tables S5 and S6). In fact, in all the studied cases the $WVTR_{(n)}$ of the reference sample (PLA) (19.0 g m^{-2}/24 h), which is consistent with literature data [50], remained the highest value observed. The poor water vapour barrier property of PLA is widely known especially considering its higher water affinity than that of other polymer materials as polyolefins and polyethylentherephtalate [51,52]. Several recent works have investigated the possible incorporation of different biobased waxes in order to improve the water vapour barrier property of the final material. In particular, beeswax [53] and carnauba wax [54] have been used working with low ponderal addition and multilayer different designs. Beeswax was added in a range between 0.5 wt% and 2.5 wt%, and has allowed to obtain similar effect with respect to that observed with cutin in this study. Differently from these previous articles, the main purpose of this work is to decrease the water affinity of the composites, exploiting the waxy nature of cutin considering higher addition ratios and simpler melt blending processing. Recently [55], the water vapour permeability of PLA/bamboo fibres has been investigated, and the increasing of the bamboo fibres content determined a significant increase of the WVTR. This behaviour, which can commonly be ascribed to the hydrophilicity of fibre surfaces and to the presence of voids at the polymer-fibres interfaces, in our case was not observed suggesting a better interaction between cutin and PLA with respect to that between PLA and bamboo. However, regarding the addition of raw cutin it was observed that PLA Cut5 showed the lowest value of the series, while the $WVTR_{(n)}$ of PLA Cut10 was slightly higher and that of PLA Cut20 increased to 17.4 g m^{-2}/24 h. This trend may be due to the presence of inhomogeneity of the cutin distribution into the composite bulk structure. The effect of these inhomogeneities was negligible with the addition of 5 wt% but became important for major cutin ponderal amounts, as it is also possible to observe on the sample films (Fig. 9). Measurements of water vapour permeability on the composites of PLA and ground cutin, PLA Mac10 and PLA Mac20, showed lower values of $WVTR_{(n)}$ than PLA Cut10 and PLA Cut20, respectively. The decreasing of the water vapour transmission rate and permeability on the last composites, which is comparable to that of PLA Cut5, may imply a better dispersion of ground cutin compared to the raw one on the bulk of the materials. The pre-grinding procedure, therefore, increases the surface area of the raw cutin and reduces the presence of the agglomeration, thus improving the interaction between cutin and PLA and also reducing the size of the remained agglomerates. From the point of view of water vapour permeability, it seems that to obtain films containing significant cutin ponderal amount and preserving the low water permeability obtained, the best strategy is to use pre-ground material instead of a coarse one.

4. Conclusions

In this work, lyophilized (Cut), and lyophilized pre-ground (Mac) cutin from tomato peel wastes were used for the preparation of blends (amount of cutin from 5 to 20 wt%) with poly(lactic acid).

The analyses performed on cutin highlighted the linear/branched nature of the THF soluble fraction (Cut Ext) and the crosslinked one of the residues (Cut Res). Regarding Cut Res, it is possible to observe predominantly the peak of C═O stretching at 1725 cm^{-1}, the absence of melting phenomena and a superior thermal stability compared to original cutin. These results were consistent with a 3D crosslinked network. Regarding Cut Ext, a lower T_g value (−21.5 °C), a split melting peak and a lower thermal stability were consistent with a simpler structure and a shorter chains length. The structural characterization of Cut Ext performed by means of NMR spectroscopy pointed to the presence of a complex matrix composed by low molecular weight species and by a supramolecular structure mainly based on long alkyl chains bearing hydroxyl functional groups, both free and esterified.

The torque of the blend showed a significant reduction compared to PLA; the same trend was observed for PLA average molecular weight, for which a decrease between 35% and 70% was observed depending on the amount of cutin present. As far as the rheological data, a decrease of the viscosity was observed in blends containing 5 wt% and 10 wt% of cutin. Interestingly, the samples containing the highest amount of cutin (20 wt %) showed a higher complex viscosity in the low-frequency region, even with respect to the PLA alone. This result was associated to the effect of a 3D network. The films obtained from the blends were subjected to water vapour permeability analyses, which pointed out that an 8%–21% reduction was obtained in the presence of 20% in weight of cutin.

The presence of the cutin also affected the cold crystallization of PLA, probably due to an increase of the hindrance among the chains. Furthermore, the cutin seemed to affect the melting of the blends. These two effects can be ascribed to the double nature of the cutin: its soluble fraction, in fact, may act as plasticizer while the insoluble one may affect the crystallization, hindering the chains and/or acting also as nucleating agent.

It is worth to note that the use of a ground cutin (Mac) could be associated to a higher final torque, a higher molecular weight and a higher complex viscosity with respect to the raw cutin (Cut). Indeed, the pre-grinding determined an increase of the surface area, together with a reduction of the size of the agglomerates, which allowed a tighter interaction with PLA.

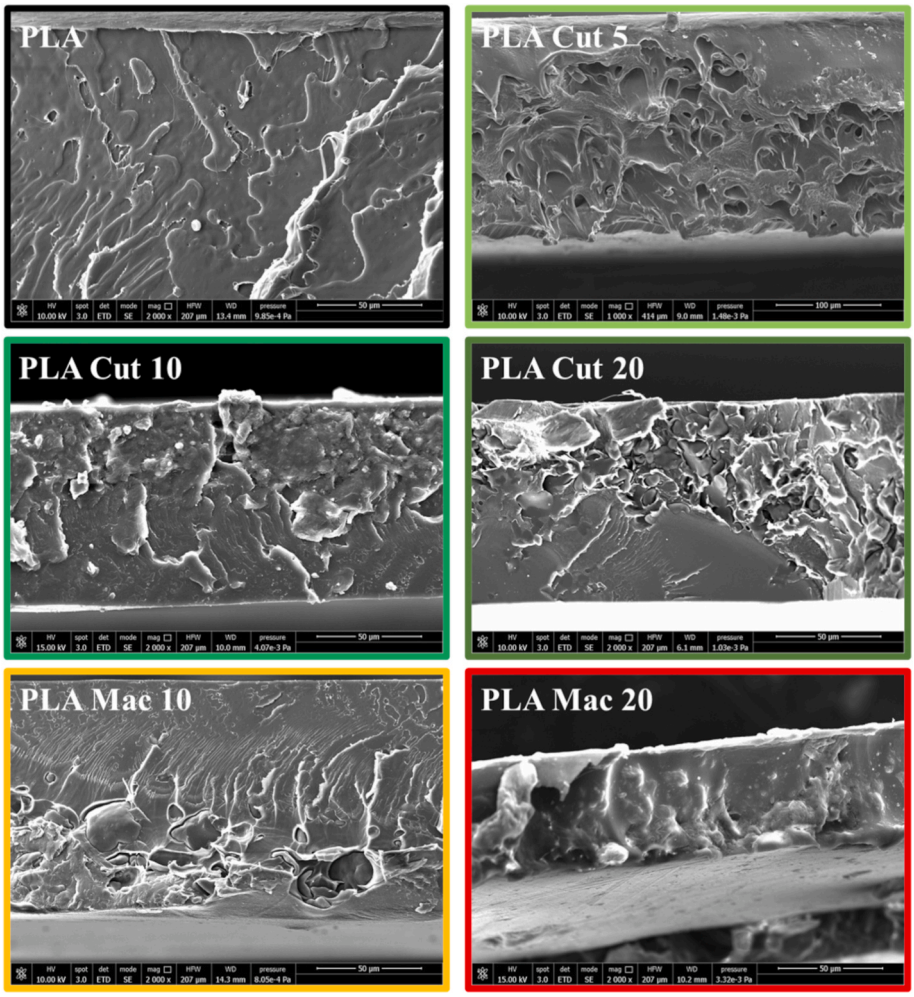

Fig. 10. SEM micrographs of PLA, PLA/Cut and PLA/Mac blends.

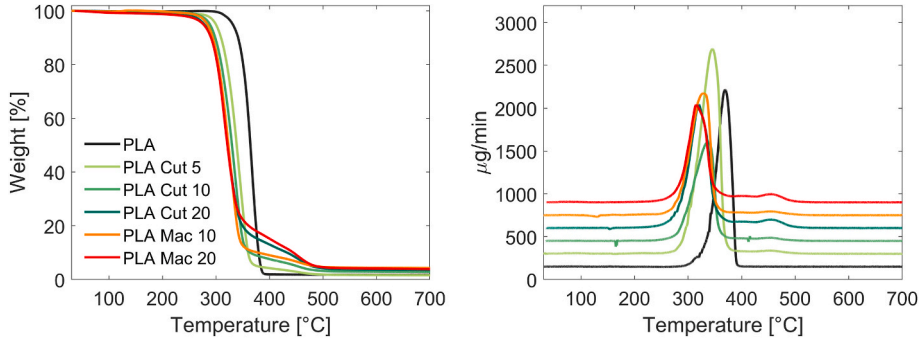

Fig. 11. TGA of PLA, PLA Cut and PLA/Mac blends (left) and their derivative DTG (right).

Table 2
Comparison of TGA and DTG results of PLA, PLA Cut and PLA/Mac blends.

Samples	From TGA		From DTG	
	T_{onset} (°C)	Residue %	T_{max} (°C)	Other Peaks (°C)
PLA	346.4	1.9	368.9	–
PLA Cut5	317.1	1.9	344.1	454.2
PLA Cut10	303.4	2.8	336.5	453.8
PLA Cut20	295.9	3.5	319.4	457.6
PLA Mac10	297.3	4.3	327.2	453.9
PLA Mac20	294.5	3.9	314.4	455.5

In conclusion, it is possible to state that the cutin extracted from tomato peels can be used as an additive in melt blending with poly(lactic acid). The degradation observed is not negligible, but considering the results achieved and the common temperature required for PLA materials, these phenomena do not compromise the processability of the blends. The experimental data highlight how it is possible to modulate the properties of the prepared materials by varying the used quantity of cutin. Further developments of this work may take into account the use of multiple different polymer matrices (e.g., PBS, PBSA, PBAT) and the evaluation of the addition of low amounts of catalysts during the process, in order to improve the extent of interactions between PLA and

Table 3
Comparison of DSC results of PLA, PLA/Cutin and PLA/Mac blends from second heating scan.

Samples	$T_{g\ cutin}$ (°C)	$T_{g\ PLA}$ (°C)	T_{cc} (°C)	ΔH_{cc} (J/g)	T_{m1} (°C)	T_{m2} (°C)	ΔH_m (J/g)	χ%[a]
PLA	–	58.5 ± 0.1	115.8 ± 0.1	−23.6 ± 0.2	148.4 ± 0.2	–	28 ± 1	5 ± 1
PLA Cut5	n.d.	55.8 ± 0.1	123.0 ± 0.4	−18.8 ± 0.4	149.2 ± 0.3	–	25.2 ± 0.6	7.2 ± 0.7
PLA Cut10	−8.3 ± 0.2	54.2 ± 0.2	117.3 ± 0.1	−26.9 ± 0.7	147.1 ± 0.4	153.1 ± 0.2	34.2 ± 0.8	9 ± 1
PLA Cut20	−9.3 ± 0.4	53.0 ± 0.5	114.3 ± 0.1	−24.7 ± 0.5	144.8 ± 0.3	152.0 ± 0.3	32 ± 1	10 ± 1
PLA Mac10	−6.1 ± 0.5	55.1 ± 0.8	119.8 ± 0.8	−25.2 ± 0.6	148.3 ± 0.7	153.1 ± 0.5	29.9 ± 0.7	6 ± 1
PLA Mac20	−6.4 ± 0.2	53.6 ± 0.5	120.7 ± 0.3	−19.3 ± 0.3	147.7 ± 0.4	153.1 ± 0.4	25.3 ± 0.4	8.0 ± 0.5

[a] χ% calculated with Equation (1) (ΔH°_m = 93.6 J/g).

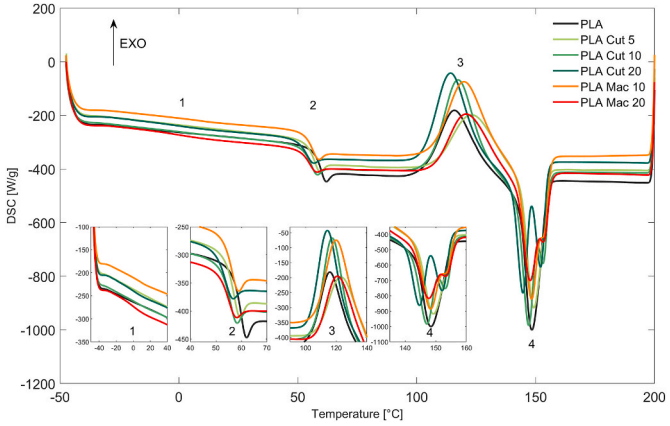

Fig. 12. Comparison between second heating of PLA, PLA/Cutin and PLA/Mac blends and magnifications.

Table 4
Water vapour permeability results of PLA, PLA/Cutin and PLA/Mac blends (T = 23 °C and relative humidity of 50 %).

Samples	WVTR (g m^{-2}/24 h)	$WVTR_{(n)}$ (g m^{-2}/24 h)	Permeability g mm m^{-2}/(24 h mmHg)
PLA	13.4 ± 0.2	19.0 ± 0.3	0.217 ± 0.003
PLA Cut5	18.2 ± 0.02	15.1 ± 0.02	0.173 ± 0.0002
PLA Cut10	17.1 ± 0.2	15.7 ± 0.2	0.179 ± 0.002
PLA Cut20	17.4 ± 0.2	17.4 ± 0.2	0.199 ± 0.003
PLA Mac10	19.7 ± 0.2	14.8 ± 0.1	0.169 ± 0.002
PLA Mac20	16.4 ± 0.5	15.0 ± 0.5	0.171 ± 0.006

cutin itself.

Funding

This work was made possible with funding received from the Bio Based Industries Joint Undertaking under the European Union's Horizon 2020 research and innovation programme, under Grant Agreement N. 720719, Agrimax project.

CRediT authorship contribution statement

L. Arrighetti: Writing – review & editing, Writing – original draft, Software, Methodology, Formal analysis, Data curation. **L. Ricci:** Writing – review & editing, Software, Methodology, Formal analysis, Data curation, Conceptualization. **C. De Monte:** Writing – review & editing, Software, Methodology, Formal analysis, Data curation, Conceptualization. **F. Aiello:** Writing – review & editing, Writing – original draft, Visualization, Validation, Methodology, Investigation, Formal analysis, Data curation. **C.A. Massa:** Writing – review & editing, Software, Methodology. **F. Balzano:** Writing – review & editing, Writing – original draft, Validation, Methodology, Formal analysis, Data curation. **G. Uccello Barretta:** Writing – review & editing, Writing – original draft, Validation, Resources, Methodology. **S. Bronco:** Writing – review & editing, Supervision, Resources, Methodology, Funding acquisition, Conceptualization.

Declaration of competing interest

The authors declare that they have no known competing financial interests or personal relationships that could have appeared to influence the work reported in this paper.

Data availability

Data will be made available on request.

Acknowledgments

The authors would like to thank "Azienda Agricola Chiesa Virginio", Canneto sull'Oglio and SSICA (Stazione Sperimentale per l'Industria delle Conserve Alimentari) for the preparation of the cutin from tomato peels waste. The authors thank Luca Pardi (CNR-IPCF) for the revision of the English language of the manuscript.

Appendix A. Supplementary data

Supplementary data to this article can be found online at https://doi.org/10.1016/j.mtsust.2024.100852.

References

[1] PlasticsEurope, Plastics-the Facts 2020 an analysis of European plastics production, demand and waste data. https://plasticseurope.org/knowledge-hub/plastics-the-facts-2020/, 2020. (Accessed 9 November 2023).
[2] Statista, Plastic waste flow worldwide in 2016 with a forecast to 2040 under business-as-usual scenario, by treatment, 2020. https://www.statista.com/statistics/1270092/plastic-waste-treatment-and-disposal-projections-worldwide/. (Accessed 20 June 2023).
[3] A.H.D. Abdullah, A.K. Fikriyyah, O.D. Putri, P.P. Puspa Asri, Fabrication and characterization of poly lactic acid (PLA)-Starch based bioplastic composites, in: IOP Conf Ser Mater Sci Eng 553, Institute of Physics Publishing, 2019, https://doi.org/10.1088/1757-899X/553/1/012052, 012052.
[4] M.M. Hassan, M.J. Le Guen, N. Tucker, K. Parker, Thermo-mechanical, morphological and water absorption properties of thermoplastic starch/cellulose composite foams reinforced with PLA, Cellulose 26 (2019) 4463–4478, https://doi.org/10.1007/s10570-019-02393-1.
[5] L. Suryanegara, A.N. Nakagaito, H. Yano, Thermo-mechanical properties of microfibrillated cellulose-reinforced partially crystallized PLA composites, Cellulose 17 (2010) 771–778, https://doi.org/10.1007/s10570-010-9419-5.
[6] H.A. Abba, I.Z. Nur, S.M. Salit, Review of agro waste plastic composites production, J. Miner. Mater. Char. Eng. 1 (2013) 271–279, https://doi.org/10.4236/jmmce.2013.15041.
[7] M.S. Lopes, A.L. Jardini, R.M. Filho, Synthesis and characterizations of poly (lactic acid) by ring-opening polymerization for biomedical applications, Chem Eng Trans 38 (2014) 331–336, https://doi.org/10.3303/CET1438056.
[8] W.H. Wan Ishak, N.A. Rosli, I. Ahmad, Influence of amorphous cellulose on mechanical, thermal, and hydrolytic degradation of poly(lactic acid) biocomposites, Sci. Rep. 10 (2020) 11342–11355, https://doi.org/10.1038/s41598-020-68274-x.
[9] A. Maqbool, S. Khan, A. Haleem, M.I. Khan, in: H. Kumar, P. Jain (Eds.), Recent Advances in Mechanical Engineering. Lecture Notes in Mechanical Engineering, Springer, 2020, pp. 147–160, https://doi.org/10.1007/978-981-15-1071-7_14.

[10] W.R. Stahel, The circular economy, Nature 531 (2016) 435–438, https://doi.org/10.1038/531435a.
[11] C. De Monte, L. Arrighetti, L. Ricci, A. Civello, S. Bronco, Agro-waste bean fibers as reinforce materials for polycaprolactone composites, Compounds 3 (2023) 504–520, https://doi.org/10.3390/compounds3030036.
[12] United Nations Environment Programme, Food Waste Index Report 2021, Nairobi, 2021. No: 978-92-807-3868-1.
[13] S.K. Amit, M.M. Uddin, R. Rahman, S.M.R. Islam, M.S. Khan, A review on mechanisms and commercial aspects of food preservation and processing, Agric. Food Secur. 6 (2017), https://doi.org/10.1186/s40066-017-0130-8.
[14] M. Crino, T. Barakat, H. Trevena, B. Neal, Systematic review and comparison of classification frameworks describing the degree of food processing, Nutr. Food Technol. 3 (2017) 1–12, https://doi.org/10.16966/2470-6086.138.
[15] J.P. Trigo, E.M.C. Alexandre, J.A. Saraiva, M.E. Pintado, High value-added compounds from fruit and vegetable by-products–Characterization, bioactivities, and application in the development of novel food products, Crit. Rev. Food Sci. Nutr. 60 (2019) 1388–1416, https://doi.org/10.1080/10408398.2019.1572588.
[16] L.L. Del Rio Osorio, E. Flórez-López, C.D. Grande-Tovar, The potential of selected agri-food loss and waste to contribute to a circular economy: applications in the food, cosmetic and pharmaceutical industries, Molecules 26 (2021) 515–557, https://doi.org/10.3390/molecules26020515.
[17] Statista, Global production of vegetables in 2020, by type. https://www.statista.com/statistics/264065/global-production-of-vegetables-by-type/. (Accessed 20 June 2023).
[18] M.R. Ventura, M.C. Pieltain, J.I.R. Castanon, Evaluation of tomato crop by-products as feed for goats, Anim. Feed Sci. Technol. 154 (2009) 271–275, https://doi.org/10.1016/j.anifeedsci.2009.09.004.
[19] M. Del Valle, M. Cámara, M.E. Torija, Chemical characterization of tomato pomace, J. Sci. Food Agric. 86 (2006) 1232–1236, https://doi.org/10.1002/jsfa.2474.
[20] H. Al-Wandawi, M. Abdul-Rahman, K. Al-Shaikhly, Tomato processing wastes as essential raw materials source, J. Agric. Food Chem. 33 (1985) 804–807, https://doi.org/10.1021/jf00065a009.
[21] P.S.N. Chada, P.H. Santos, L.G.G. Rodrigues, G.A.S. Goulart, J.D. Azevedo dos Santos, M. Maraschin, M. Lanza, Non-conventional techniques for the extraction of antioxidant compounds and lycopene from industrial tomato pomace (Solanum lycopersicum L.) using spouted bed drying as a pre-treatment, Food Chem. X. 13 (2022) 100237, https://doi.org/10.1016/j.fochx.2022.100237.
[22] A.M. Giuffrè, M. Capocasale, C. Zappia, M. Poiana, Biodiesel from tomato seed oil: transesterification and characterisation of chemical-physical properties, Agron. Res. 15 (2017) 133–143.
[23] A. Cifarelli, I.M. Cigognini, L. Bolzoni, A. Montanari, Physical-chemical characteristics of cutin separated from tomato waste for the preparation of bio-lacquers, Adv. Mater. Sci. Eng. 11 (2019) 33–45, https://doi.org/10.32732/ase.2019.11.1.33.
[24] A. Heredia, Biophysical and biochemical characteristics of cutin, a plant barrier biopolymer, Biochim. Biophys. Acta Gen. Subj. 1620 (2003) 1–7, https://doi.org/10.1016/S0304-4165(02)00510-X.
[25] T.J. Walton, P.E. Kolattukudy, Determination of the structures of cutin monomers by a novel depolymerization procedure and combined gas chromatography and mass spectrometry, Biochemistry 11 (1972) 1885–1897, https://doi.org/10.1021/bi00760a025.
[26] J.J. Benítez, J.A. Heredia-Guerrero, S. Guzmán-Puyol, M.J. Barthel, E. Domínguez, A. Heredia, Polyhydroxyester films obtained by non-catalyzed melt-polycondensation of natural occurring fatty polyhydroxyacids, Front. Mater. 2 (2015), https://doi.org/10.3389/fmats.2015.00059.
[27] J.A. Heredia-Guerrero, J.J. Benítez, P. Cataldi, U.C. Paul, M. Contardi, R. Cingolani, I.S. Bayer, A. Heredia, A. Athanassiou, All-natural sustainable packaging materials inspired by plant cuticles, Adv. Sustain. Syst. 1 (2017) 1600024, doi: 10.1002/adsu.201600024.
[28] BIOCOPACplus Sustainable bio-based coating from tomato processing by-products for food metal packaging. https://biocopacplus.eu/. (Accessed 31 August 2023).
[29] K. Yu, D. Wang, J. Hou, X. Zhang, J. Chen, Fabrication of poly(lactic acid) foam with high expansion ratio and oriented cellular structure by restricting cold crystallization, Int. J. Biol. Macromol. 251 (2023) 126463, https://doi.org/10.1016/j.ijbiomac.2023.126463.
[30] T. Isaacson, D.K. Kosma, A.J. Matas, G.J. Buda, Y. He, B. Yu, A. Pravitasari, J. D. Batteas, R.E. Stark, M.A. Jenks, J.K.C. Rose, Cutin deficiency in the tomato fruit cuticle consistently affects resistance to microbial infection and biomechanical properties, but not transpirational water loss, Plant J. 60 (2009) 363–377, https://doi.org/10.1111/j.1365-313X.2009.03969.x.
[31] J.A. Heredia-Guerrero, J.J. Benítez, E. Domínguez, I.S. Bayer, R. Cingolani, A. Athanassiou, A. Heredia, Infrared and Raman spectroscopic features of plant cuticles: a review, Front. Plant Sci. 5 (2014) 1–14, https://doi.org/10.3389/fpls.2014.00305.
[32] E. Dominguez, J.A. Heredia-Guerrero, A. Heredia, The biophysical design of plant cuticles: an overview, New Phytol. 189 (2011) 938–949, https://doi.org/10.1111/j.1469-8137.2010.03553.x.
[33] A. Manrich, F.K.V. Moreira, C.G. Otoni, M.V. Lorevice, M.A. Martins, L.H. C. Mattoso, Hydrophobic edible films made up of tomato cutin and pectin, Carbohydr. Polym. 164 (2017) 83–91, https://doi.org/10.1016/j.carbpol.2017.01.075.
[34] J.J. Benítez, P.M. Castillo, J.C. Del Río, M. León-Camacho, E. Domínguez, A. Heredia, S. Guzmán-Puyol, A. Athanassiou, J.A. Heredia-Guerrero, Valorization of tomato processing by-products: fatty acid extraction and production of bio-based materials, Materials 11 (2018) 2211–2224, https://doi.org/10.3390/ma11112211.
[35] J.A. Heredia-Guerrero, G. Caputo, S. Guzman-Puyol, G. Tedeschi, A. Heredia, L. Ceseracciu, J.J. Benitez, A. Athanassiou, Sustainable polycondensation of multifunctional fatty acids from tomato pomace agro-waste catalyzed by tin (II) 2-ethylhexanoate, Mater. Today Sustain. 3–4 (2019) 100004, https://doi.org/10.1016/j.mtsust.2018.12.001.
[36] J.J. Benítez, A. González Moreno, S. Guzmán-Puyol, J.A. Heredia-Guerrero, A. Heredia, E. Domínguez, The response of tomato fruit cuticle membranes against heat and light, Front. Plant Sci. 12 (2022), https://doi.org/10.3389/fpls.2021.807723.
[37] S.A. Chaudhari, R.S. Singhal, Cutin from watermelon peels: A novel inducer for cutinase production and its physicochemical characterization, Int. J. Biol. Macromol. 79 (2015) 398–404, https://doi.org/10.1016/j.ijbiomac.2015.05.006.
[38] L.A. García-Zapateiro, J.M. Franco, C. Valencia, M.A. Delgado, C. Gallegos, M. V. Ruiz-Méndez, Chemical, thermal and viscous characterization of high-oleic sunflower and olive pomace acid oils and derived estolides, Grasas Aceites 64 (2013) 497–508, https://doi.org/10.3989/gya.012513.
[39] M.C. Righetti, P. Cinelli, N. Mallegni, C.A. Massa, S. Bronco, A. Stäbler, A. Lazzeri, Thermal, mechanical, and rheological properties of biocomposites made of poly (lactic acid) and potato pulp powder, Int. J. Mol. Sci. 20 (2019) 675, https://doi.org/10.3390/ijms20030675.
[40] Y. Zare, V. Mišković-Stanković, K.Y. Rhee, The complex viscosity of polymer carbon nanotubes nanocomposites as a function of networks properties, Carbon Letters 29 (2019) 535–545, https://doi.org/10.1007/s42823-019-00050-y.
[41] B. Wang, T. Wan, W. Zeng, Dynamic rheology and morphology of polylactide/organic montmorillonite nanocomposites, J. Appl. Polym. Sci. 121 (2011) 1032–1039, https://doi.org/10.1002/app.33717.
[42] V. Speranza, A. De Meo, R. Pantani, Thermal and hydrolytic degradation kinetics of PLA in the molten state, Polym. Degrad. Stabil. 100 (2014) 37–41, https://doi.org/10.1016/j.polymdegradstab.2013.12.031.
[43] M. Zhou, P. Zhou, P. Xiong, X. Qian, H. Zheng, Crystallization, rheology and foam morphology of branched PLA prepared by novel type of chain extender, Macromol. Res. 23 (2015) 231–236, https://doi.org/10.1007/s13233-015-3018-0.
[44] Y. Zare, S.P. Park, K.Y. Rhee, Analysis of complex viscosity and shear thinning behavior in poly (lactic acid)/poly (ethylene oxide)/carbon nanotubes biosensor based on Carreau–Yasuda model, Results Phys. 13 (2019) 102245, https://doi.org/10.1016/j.rinp.2019.102245.
[45] C. McCurdy, D. Dixion, E. Archer, T. Dooher, I. Edwards, A Comparison of the sealing, forming and moisture vapour transmission properties of polylactic acid (PLA), polyethene (PE) and polyethylene terephthalate (PET) coated boards for packaging applications, J. Packag. Technol. Res. 6 (2022) 91–100, https://doi.org/10.1007/s41783-022-00131-w.
[46] Z. Duan, N.L. Thomas, W. Huang, Water vapour permeability of poly(lactic acid) nanocomposites, J. Membr. Sci. 445 (2013) 112–118, https://doi.org/10.1016/j.memsci.2013.06.008.
[47] Z. Duan, N.L. Thomas, Water vapour permeability of poly(lactic acid): crystallinity and the tortuous path model, J. Appl. Phys. 115 (2014) 064903, https://doi.org/10.1063/1.4865168.
[48] H. Tsuji, R. Okino, H. Daimon, K. Fujie, Water vapor permeability of poly(lactide)s: effects of molecular characteristics and crystallinity, J. Appl. Polym. Sci. 99 (2006) 2245–2252, https://doi.org/10.1002/app.22698.
[49] G.L. Siparsky, K.J. Voorhees, J.R. Dorgan, K. Schilling, Water Transport in Polylactic Acid (PLA), PLA/Polycaprolactone Copolymers, and PLA/Polyethylene Glycol Blends, J. Environ. Polym. Degrad. 5 (1997) 125–136, https://doi.org/10.1007/BF02763656.
[50] Z.J. Chen, C.H. Tsou, M.L. Tsai, J. Guo, M.R. De Guzman, T. Yang, C. Gao, Y. Lei, P. W. Gan, S. Chen, L.J. Tu, C.L. Qu, R.Y. Wang, C.S. Wu, Barrier properties and hydrophobicity of biodegradable poly(Lactic acid) composites reinforced with recycled Chinese spirits distiller's grains, Polymers 13 (2021) 2861, https://doi.org/10.3390/polym13172861.
[51] A.M. LaChance, Z. Hou, M.M. Farooqui, S.A. Carr, J.M. Serrano, C.E. Odendahl, M. E. Hurley, T.E. Morrison, J.L. Kubachka, N.T. Samuels, A.T. Barrett, Y. Zhao, A. M. DeGennaro, M.H. Camara, L. Sun, Polyolefin films with outstanding barrier properties based on one-step coassembled nanocoatings, Adv. Compos. Hybrid Mater. 5 (2022) 1067–1077, https://doi.org/10.1007/s42114-022-00421-6.
[52] C. Zhu, J. Yin, Z. Zhang, F. Shi, Bio-based poly(ethylene furanoate)/ZnO transparent thin films with improved water vapor barrier and antibacterial properties for food packaging application, Mater. Res. Express 9 (2022) 115304, https://doi.org/10.1088/2053-1591/aca3fc.
[53] J.H. Lim, J.A. Kim, J.A. Ko, H.J. Park, Preparation and characterization of composites based on polylactic acid and beeswax with improved water vapor barrier properties, J. Food Sci. 80 (2015) E2471–E2477, https://doi.org/10.1111/1750-3841.13081.
[54] E. Pasquier, B.D. Mattos, H. Koivula, A. Khakalo, M.N. Belgacem, O.J. Rojas, J. Bras, Multilayers of renewable nanostructured materials with high oxygen and water vapor barriers for food packaging, ACS Appl. Mater. Interfaces 14 (2022) 30236–30245, https://doi.org/10.1021/acsami.2c07579.
[55] C.S. Wu, D.Y. Wu, S.S. Wang, Preparation and characterization of polylactic acid/bamboo fiber composites, ACS Appl. Bio Mater. 5 (2022) 1038–1046, https://doi.org/10.1021/acsabm.1c01082.